HYBRID MAGNETICALLY SEPARABLE CATALYST FOR THE HYDROGENATION OF LEVULINIC ACID TO γ-VALEROLACTONE

Cite this: *INEOS OPEN*, **2023**, *6 (4)*, 119–125
DOI: 10.32931/io2320a

Received 12 December 2023,
Accepted 16 January 2024

http://ineosopen.org

S. A. Sorokina,[a] M. E. Grigor'ev,[b] N. V. Kuchkina,[a] A. S. Torozova,[a] L. Zh. Nikoshvili,[b] M. G. Sul'man,[b] and Z. B. Shifrina*[a]

[a] *Nesmeyanov Institute of Organoelement Compounds, Russian Academy of Sciences, ul. Vavilova 28, str. 1, Moscow, 119334 Russia*
[b] *Tver State Technical University, nab. Afanasiya Nikitina 22, Tver, 170026 Russia*

Abstract

Catalytic hydrogenation of plant-derived levulinic acid (LA) to γ-valerolactone (GVL) is a promising way for obtaining liquid fuels by sustainable methods. This work deals with the synthesis of a hybrid organic–inorganic ruthenium catalyst that showed high activity and stability in the production of GVL. A combination of an organic phase, namely, a layer of a branched pyridylphenylene polymer that uniformly distributes the catalytic complexes over a substrate, and an inorganic carrier SiO_2 with magnetic nanoparticles, which has a hydrophilic surface, allowed for accomplishing the reaction in water and provided GVL in a quantitative yield for 180 min at 150 °C and 2 MPa or for 60 min at 150 °C and 5 MPa. Owing to simple recovery through magnetic separation, the catalyst was used in six catalytic runs without a significant decrease in the activity.

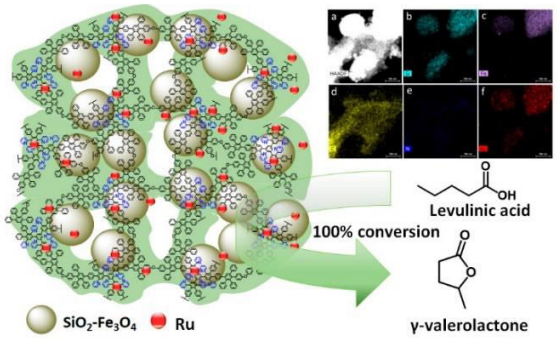

Key words: levulinic acid, γ-valerolactone, ruthenium, nanoparticles, heterogeneous catalysis.

Introduction

Progress in the development of chemical science is inextricably connected with the development and improvement of modern catalytic systems. Traditionally, catalysts are divided into homogeneous, which are in the same phase with reacting compounds, and heterogeneous, which do not dissolve in the reaction mixture. Homogeneous catalysts commonly consist of an organic ligand which coordinates and stabilizes metal center atoms and exhibit high activity and selectivity. However, their industrial application is limited due to the impossibility of recycling, difficulty of isolation, and contamination of the target product. In contrast, heterogeneous catalysts can be easily recovered from the reaction mixture, regenerated and recycled; however, they are significantly inferior in the activity and selectivity to homogeneous catalysts. One of the most commonly used methods for heterogenization is the application of a metal on a substrate, such as SiO_2, Al_2O_3, TiO_2, ZrO_2, *etc*.

At the same time, the creation of hybrid organic–inorganic systems allows for joining together the advantages of both classes of catalysts, combine the possibility of repeated use with high activity in one composite [1, 2]. In such systems, organic and inorganic phases are combined on a nanometer and sub-micrometer scale, and the structural features are not just the sum of individual components, but the result of their interaction and mutual influence [3]. Organic and inorganic phases, as a rule, are covalently bound with each other, most often through an oxygen-containing functional group [4, 5]. Nitrogen- and sulfur-containing groups are also used to form spacers [6]. In this case, the organic part serves to stabilize and coordinate the metal center, while the inorganic part ensures separation of the catalyst from the reaction mixture [4, 7].

Such systems are created using graphene, carbon nitride, carbon nanotubes, silica gel, and other materials [8–12]. This approach leads to the most efficient use of a metal owing to its high dispersion on the substrate. At the same time, there remains a danger of aggregation of metal centers if stabilization is not sufficient. Therefore, when designing hybrid catalytic systems, the organic ligand, in addition to coordinating the metal atom, must create steric hindrances that prevent the aggregation of catalytic particles and also form a barrier to leaching of the metal into the reaction medium. In this respect, hybrid catalysts based on dendritic ligands have become widespread. These systems were obtained based on poly(propyleneimine), poly(amidoamine), polylysine and other dendrimers [13–19]. However, these types of dendrimers are flexible molecules and their chains are capable of the so-called backfolding, *i.e.*, can fold and change their conformation, thereby hindering access for reacting molecules to the catalytic centers. An attractive alternative to flexible-chain dendrimers are rigid-chain molecules with limited torsional rotation around bonds that retain their branched architecture regardless of a solvent, temperature, and other conditions. These compounds include fully aromatic pyridylphenylene dendrimers, which feature constant shape, thermal and chemical stability, and high rigidity [20].

Earlier, hybrid magnetically separable palladium-containing catalysts have been developed using pyridylphenylene dendrons that showed high catalytic activity in the Suzuki and Sonogashira cross-coupling in an aqueous medium for a series

of model aryl bromide substrates [21–23]. The presence of a magnetic component (Fe_3O_4 nanoparticles) ensured the reduction of material costs, since effective magnetic separation of the catalyst after the reaction practically did not reduce its activity in subsequent catalytic cycles. The pyridyl-containing dendritic ligands effectively stabilized Pd nanoparticles and complexes, preventing the catalyst loss in reactions and making active sites accessible to substrates. The approach to the synthesis of these systems was based on the sequential design of catalytic systems, consisting of several stages: the dendron synthesis, functionalization of silica gel surface, and cross-linking of organic and inorganic phases. In order to reduce material and energy costs, we developed a new method for the formation of hybrid catalytic systems, based on the application of a layer of hyperbranched pyridylphenylene polymer (HPP) on an inorganic support: SiO_2 and Al_2O_3 [24]. The polycondensation of two monomers in the presence of the inorganic phase was accompanied by the formation of a cross-linked branched polymeric structure on the substrate surface, additionally stabilized by hydrogen bonds between the pyridine units included in the polymer and the hydroxy groups on the surface of the oxide substrate. The coordination of the resulting composite with palladium acetate afforded a catalytic system that exhibited higher activity in the Suzuki cross-coupling between bromobenzaldehyde and phenylboronic acid than the earlier published analogs [24]. The suggested approach also appeared to be effective for creating the catalysts that show high activity in the hydrogenation of CO_2 into methanol [25]. The activity of the catalyst was superior to the commercially available analog and remained at a high level over several catalytic runs.

In this work, we studied the activity of hybrid composites based on SiO_2–Fe_3O_4–HPP in the hydrogenation of levulinic acid (LA) to γ-valerolactone (GVL). LA, obtained by hydrolysis of lignocellulose, is an important basic compound that is utilized in the industrial production of organic acids, pesticides, solvents, *etc.* [26–28]. In particular, the hydrogenation of LA to γ-valerolactone (GVL) is one of the most promising reactions in the field of biomass processing to obtain intermediate products of fine organic synthesis and liquid fuel [29, 30]. Different heterogeneous catalysts based on Co, Cu, Ni, Pt, and Pd have been developed for this process [13, 31–35]. However, the Ru-based catalysts exhibit the highest activity [36–38]. At the same time, hybrid Ru-containing catalysts remain virtually unexplored in this reaction. Taking into account the high catalytic activity of the hybrid catalysts based on SiO_2–Fe_3O_4–HPP–M (Me = Pd, Cr) in the earlier studied processes [21–25], the investigation of these catalytic systems in the LA hydrogenation seemed to be promising. Furthermore, the high thermal stability of HPP is an additional advantage that enables the use of such systems under severe reaction conditions. In this work, a Ru^{3+} salt was applied to the SiO_2–Fe_3O_4–HPP support to form a catalytically active composite. In this case, the polymer component was responsible for the formation and stabilization of catalytic complexes, and the mesoporous substrate with magnetic nanoparticles ensured effective magnetic separation of the catalyst from the reaction mixture and reaction products and its subsequent use, as well as a large surface area.

Results and discussion

The synthesis of the catalytically active composite was accomplished in several steps. At the first stage, Fe_3O_4 nanoparticles were obtained in the pores of commercially available mesoporous SiO_2 by thermal decomposition of iron nitrate in the presence of a mild reducing agent [39]. The particle size estimated by the Debye–Scherrer equation from powder X-ray diffraction data was 13.2 nm. Magnetic nanoparticles provide easy separation of the catalyst from the reaction mixture for recycling by applying an external magnetic field. This opens the way to more environmentally benign processes, energy conservation, and cheaper target products. After the formation of the magnetic substrate, a layer of pyridylphenylene polymer was applied to its surface by the Diels–Alder polycondensation of a first-generation dendrimer with six ethynyl groups and a bis(cyclopentadienone) containing two diene bonds. The synthetic scheme for the resulting composite (SiO_2–Fe_3O_4–HPP) is presented in Fig. S1 in the Electronic supplementary information (ESI). Note that the composite unit of the polymer incorporates six pyridine rings capable of coordinating with metal salts. Thus, $RuCl_3$ was introduced into the SiO_2–Fe_3O_4–HPP substrate to form a catalytically active composite in which Ru compounds are stabilized by the matrix of the pyridine-containing polymer.

The hydrogenation of LA to GVL proceeds under severe conditions, at high temperatures and pressures. Therefore, the thermal and chemical stability of the catalyst are important aspects that determine the possibility of using a particular catalytic composite in the given reaction. It was previously shown that the temperature of the onset of thermal decomposition of SiO_2–Fe_3O_4–HPP is 510 °C, confirming the high stability of the composite [24]. The surface area of SiO_2–Fe_3O_4–HPP calculated using the BET method was 246 m^2/g [24]. After the introduction of Ru, the surface area decreased to 205 m^2/g. The liquid nitrogen adsorption–desorption isotherms of the SiO_2–Fe_3O_4–HPP–Ru catalyst are shown in Fig. S2 in the ESI. The powder X-ray diffraction data (Fig. S3 in the ESI) revealed the presence of a polymer halo in the diffraction pattern in the region of 10° 2θ, a broad signal at 22° 2θ corresponding to SiO_2, as well as a set of reflections corresponding to the spinel structure (Fe_3O_4).

The amount of ruthenium introduced into the composite, estimated based on the results of X-ray fluorescence analysis (XRF) was 3.3 wt %. Furthermore, the chemical composition of the catalyst was confirmed using energy-dispersive X-ray spectroscopy (EDS) (Fig. 1). The spectrum shows the presence of all constituent elements. The signal at 8 keV corresponds to Cu Kα emission and its presence is associated with the application of a copper grating for the spectrum registration.

The morphology and location of chemical elements in the catalyst were studied using elemental maps obtained by EDS (Fig. 2). The micrographs revealed the presence of a carbon shell distributed around silica gel particles. Iron oxide nanoparticles are located in the pores of silica gel. Ruthenium is also evenly distributed throughout the sample, with no visible aggregates, which indicates its reliable stabilization.

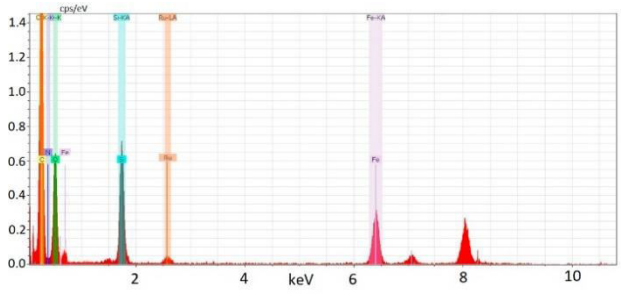

Figure 1. EDS spectrum of the SiO_2–Fe_3O_4–HPP–Ru catalyst.

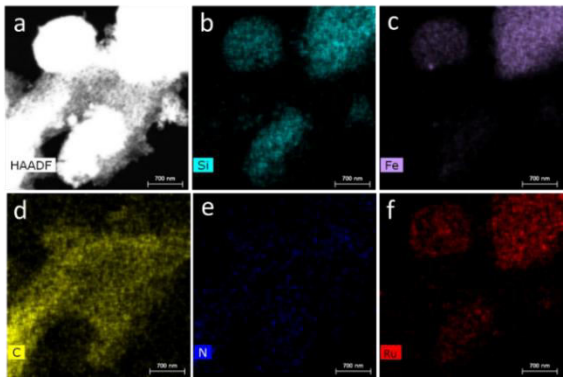

Figure 2. Dark-field image of the SiO_2–Fe_3O_4–HPP–Ru catalyst (***a***) and elemental maps for Si (***b***), Fe (***c***), C (***d***), N (***e***), and Ru (***f***).

The valence state of the metals was studied using X-ray photoelectron spectroscopy (XPS). Figure 3a shows the Fe 2p XPS spectrum. The spectrum deconvolution revealed the presence of Fe^{2+} and Fe^{3+} compounds with peaks located at 710.4 and 712.2 eV for $2p_{3/2}$ Fe^{2+} and Fe^{3+}, respectively. In this case, the presence of a plateau between the Fe^{2+} and Fe^{3+} peaks indicates the formation of Fe_3O_4. Otherwise (in the case of the formation of Fe_2O_3), the predominance of Fe^{3+} would be reflected in the appearance of an additional peak related to the satellite, with a binding energy higher than the main peak by 8 eV.

The analysis of the N 1s spectrum (Fig. 3b) indicated the presence of a peak with a binding energy of 399.5 eV, which corresponds to the pyridine ring coordinated with the metal [40]. The data obtained confirm the complexation of the introduced ruthenium salt with pyridine units included in the polymer. The deconvolution of the high-resolution Ru XPS spectrum showed the presence of two Ru compounds. Table S1 in the ESI presents the spectrum decomposition parameters. The peak with a binding energy of 282.5 eV corresponds to $3d_{5/2}$ Ru^{3+} in $RuCl_3$. The second peak with a lower binding energy of 281.4 eV refers to $Ru(OH)_3$ or aqueous $RuCl_3$ complexes, which is a standard phenomenon for $RuCl_3$. Thus, the XPS spectrum of commercial $RuCl_3$ also demonstrates the presence of two peaks, which can be attributed to $RuCl_3$ and $Ru(OH)_3$ [41]. At the same time, in aqueous solutions $RuCl_3$ easily undergoes aquation, resulting in complexes $[RuCl_4(H_2O)_2]$, $RuCl_3(H_2O)_3$, *etc.*, as was shown earlier [42]. The presence of the second type of Ru compounds in the XPS spectrum may be associated with the use of THF as a solvent at the stage of introducing the Ru salt into the composite, as well as with the use of water-containing solvents at the stage of purification of the SiO_2–Fe_3O_4–HPP–Ru composite.

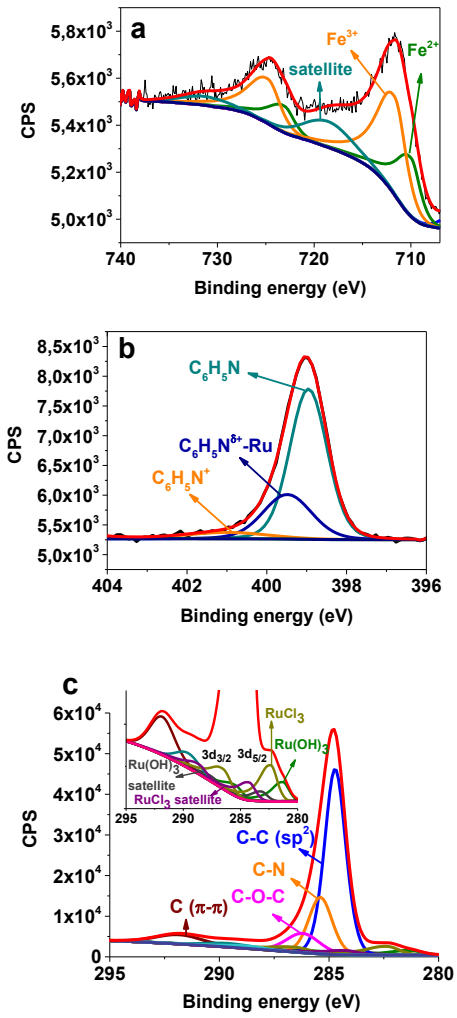

Figure 3. High-resolution XPS spectra of the SiO_2–Fe_3O_4–HPP–Ru catalyst: Fe 2p (***a***), N 1s (***b***), Ru 3d (***c***).

It is known that Ru^0 exhibits catalytic activity in the hydrogenation of LA. However, its formation can occur *in situ* during the reaction. It was shown that the activity of the catalyst reduced *in situ* was superior to that of the catalyst reduced preliminarily. *In situ* reduction occurred more efficiently in the case of hydrated ruthenium surface [43]. Taking these data into account, in this work no preliminary reduction of ruthenium was performed, and its formation occurred during the reaction.

Most often, the hydrogenation of LA to GVL is carried out in protic solvents, such as alcohol and dioxane. The use of an organic solvent, as a rule, has a beneficial effect on the yield of the target product; however, it can reduce the selectivity of the reaction due to side reactions of the solvent itself, for example, esterification or ring opening. However, the creation of a hybrid organic–inorganic catalyst allows for the hydrophilization of the catalyst surface to some extent compared to similar composites obtained only on the basis of pyridylphenylene polymers, due to the presence of hydroxy groups on the surface of silica gel. In view of this, and also considering that water is the best solvent in terms of green chemistry, in the present study, the hydrogenation of LA was carried out in water.

Temperature and pressure have strong effect on the process. The dependence of LA conversion on these parameters is presented in Fig. 4. As could be expected, a temperature rise

significantly increases the conversion of LA (Fig. 4a). Thus, at 150 °C, 100% conversion was achieved in 180 min, while at 100 °C, during the entire experiment (240 min) the conversion was 62.1%. Similarly, an increase in the pressure led to an increase in the conversion. The experiments (Fig. 4b) were carried out at a constant temperature of 120 °C. However, increasing pressure did not affect an increase in the conversion as dramatically as temperature.

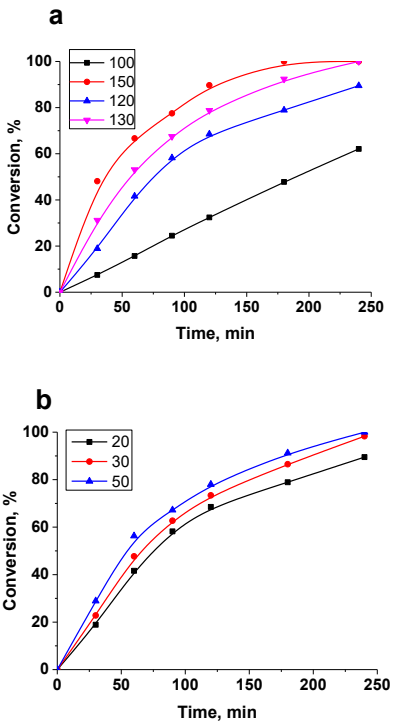

Figure 4. Effect of temperature (***a***) and pressure (***b***) on the LA conversion. The experiments were carried out at 2 MPa, the effect of pressure was studied at 120 °C.

The results of the catalytic experiments are presented in Table 1. As can be seen, the catalyst showed high activity and selectivity, affording quantitative yields of GVL. Depending on the reaction conditions, the time for 100% conversion varied from 90 to 240 min. The selectivity value averaged 99% or higher. The comparison of the catalyst under consideration with the previously developed catalysts (Table S2 in the ESI) demonstrated the effectiveness of the proposed approach.

After the reaction completion, the catalyst was separated from the reaction mixture using an external magnetic field, regenerated by washing with water, ethanol and acetone, and used in six successive catalytic runs. The results are presented in Fig. 5. The experiments were carried out under the most severe reaction conditions: 150 °C, 5 MPa. The catalyst showed excellent stability; the GVL yield after 6 catalytic runs was 95.5%.

The presence of possible changes in the catalyst after the reaction was assessed using EDS elemental maps (Fig. 6). The hydrogenation of LA was accompanied by the formation of small ruthenium nanoparticles (Fig. 6d). However, the number of particles, as well as their sizes are small, which indicates reliable stabilization of Ru by the polymer layer and ensures its high activity in the repeated tests.

Table 1. Results of the catalytic testing of SiO_2–Fe_3O_4–HPP–Ru

Entry	*T*, °C	*P*, MPa	*t*, min	Conversion, %	Selectivity, %	GVL yield, %
1	100	2	240	62.1	99.2	61.6
2	120	2	240	89.5	98.7	88.3
3	130	2	240	100	99.5	99.5
4	150	2	180	100	100	100
5	100	3	240	69.3	97.8	67.8
6	120	3	240	98.3	99.3	97.6
7	130	3	180	91.2	98.7	90.0
8	130	3	240	100	99.5	99.5
9	150	3	120	96.5	99.0	95.5
10	150	3	180	100	100	100
11	100	5	240	77.2	98.7	76.2
12	120	5	180	95.4	99.6	95.0
13	120	5	240	100	100	100
14	130	5	60	86.5	99.3	85.9
15	130	5	90	98.2	99.8	98.0
16	150	5	60	97.8	99.7	97.5
17	150	5	90	100	99.8	99.8

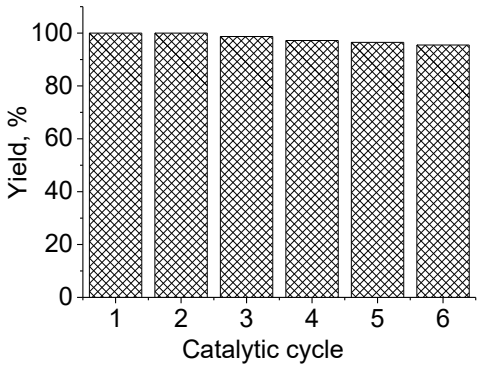

Figure 5. Results of the recycling of the SiO_2–Fe_3O_4–HPP–Ru catalyst in six catalytic runs at 150 °C, 5 MPa, and reaction time 90 min.

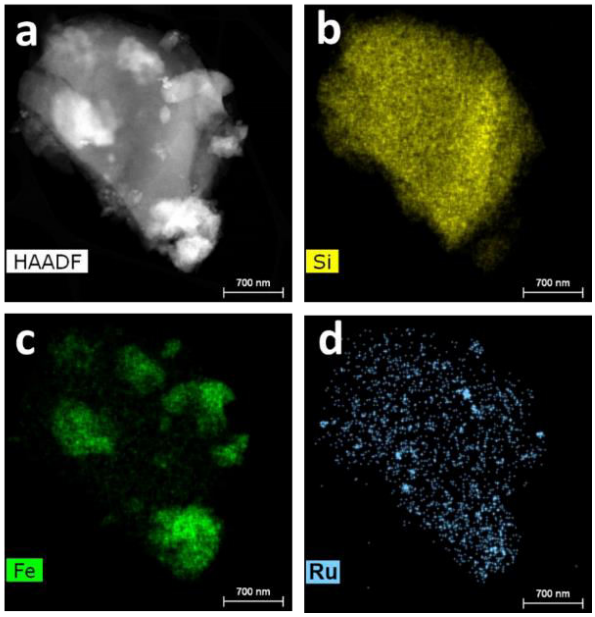

Figure 6. Dark-field image of the SiO_2–Fe_3O_4–HPP–Ru catalyst (***a***) and elemental maps for Si (***b***), Fe (***c***), and Ru (***d***) after two catalytic runs.

Experimental section

Synthesis of the catalyst

The synthesis of the SiO_2–Fe_3O_4–HPP substrate was carried out according to the earlier developed procedure [24]. For this purpose, two monomers, namely, a first-generation pyridylphenylene dendrimer bearing six ethylene groups and bis(cyclopentadienone) with two diene bonds were adsorbed on the surface of mesoporous silica gel with pre-synthesized magnetic nanoparticles. After this, a solvent (diphenyl ether) was added to the mixture, and the Diels–Alder polycondensation was carried out for 10 h. The solid was then separated from the reaction mixture using a rare-earth magnet and washed thoroughly with dichloromethane and acetone to remove unbound polymer molecules. The sample was dried in a vacuum oven and used as a substrate for introducing $RuCl_3$.

To synthesize SiO_2–Fe_3O_4–HPP–Ru, $RuCl_3$ (0.228 g) was dissolved in THF (340 mL). SiO_2–Fe_3O_4–HPP (1 g) was suspended in THF (1 L) in a round-bottom flask connected to a dropping funnel which was charged with a solution of $RuCl_3$. The complexation was carried out at room temperature during stirring for 10 h, sequentially adding the solution of $RuCl_3$ to the support. After the reaction completion, the composite was separated using a magnet and washed with THF and acetone. The sample was dried in a vacuum oven at 40 °C.

Hydrogenation of levulinic acid

LA hydrogenation was carried out in a Parr Series 5000 Multiple Reactor System (autoclave-type reactor) at a stirring speed of 1500 rpm, varying the process parameters such as temperature (100–150 °C) and partial hydrogen pressure (2–5 MPa). In a typical experiment, 0.01 g of the catalyst, 1 g of LA, and 50 mL of the solvent (distilled water) were placed in the reactor. The reactor was then sealed, purged with nitrogen (0.02 MPa), and heated under stirring. Once the selected temperature was reached, nitrogen was replaced with hydrogen, the pressure was adjusted, and the reaction began.

The samples of the reaction mixture were analyzed using a gas chromatograph (Kristallux 4000 M) equipped with an FID detector and a ZB-WAX capillary column (60 m × 0.53 mm internal diameter, film thickness 1 μm). The detector and injector temperatures were 250 °C and 300 °C, respectively. The column temperature was programmed as follows: 150 °C (13 min), heating to 230 °C (30 °C/min), and then 230 °C for 7 min. Helium (30 mL/min) was used as a carrier gas. The concentrations of the components of the reaction mixture were calculated using the absolute calibration curve method based on chemically pure components of the reaction mixture.

The LA conversion was determined as follows: X_{LA} (%) = $(C_{LA,0}–C_{LA})\cdot C_{LA,0}^{-1}\cdot 100$. The reaction selectivity was defined as follows: S_{GVL} (%) = $C_{GVL}\cdot(C_{LA,0}–C_{LA})^{-1}\cdot 100$. The GVL yield was calculated as the product of the conversion and selectivity.

For recycling experiments, the catalyst was separated from the reaction mixture, rinsed with water (500 mL), and dried in a vacuum oven at 70 °C. The subsequent catalytic reaction was carried out according to the above-described procedure.

Methods of analysis

The samples for EDS studies were prepared by immersing a copper grating with a deposited carbon layer into the SiO_2–Fe_3O_4–HPP–Ru powder. The scanning transmission electron microscopy (STEM) and EDS microanalysis were conducted on an Osiris TEM/STEM microscope (Thermo Fisher Scientific, USA), equipped with a high-angle annular dark-field detector (HAADF) (Fischione, USA) and a Super X X-ray EDS spectrometer (ChemiSTEM, Bruker, USA) at an accelerating voltage of 200 kV. The resulting images were processed using Digital Micrograph (Ga-tan, USA) and TIA (Thermo Fisher Scientific, USA) software.

The powder X-ray diffraction studies were performed with a Rigaku MiniFlex600 diffractometer (Rigaku Corporation, Japan) using Si Kα radiation (40 kV, 15 mA, Ni-Kß filter) in the angle range 2θ = 20–80° with a scan step of 0.02° and a speed of 0.5°/min. The assignment was made using PDXL software (Rigaku Corporation, Japan) and the ICDD PDF-2 database (2017).

The XPS data were obtained on an Axis Ultra DLD spectrometer (Kratos) using monochromatic Al Kα radiation. All data were obtained at an X-ray power of 150 W. The total spectra were recorded with an energy step of 1 eV at an analyzer transmission energy of 160 eV, while the high-resolution spectra were recorded with an energy step of 0.1 eV at an analyzer transmission energy of 40 eV. The samples were degassed for 180 min prior to the experiments and were stable throughout the study. The resulting data were analyzed using CasaXPS software.

The content of Ru was determined by X-ray fluorescence measurements performed on a Zeiss Jena VRA-30 spectrometer equipped with a molybdenum anode, a LiF200 analyzer, and an SD detector. The data collection time was kept constant and composed 10 s. The analysis was performed on the Ru Kα line, and a series of standards were prepared by mixing 1 g of polystyrene with 10–20 mg of the standard compounds. The elemental analyses for C, H, N, and S were obtained using a Vario Microcube microanalyzer (Elementar).

Conclusions

The creation of hybrid organic–inorganic catalysts is a promising way to construct catalytic systems owing to the combination of the principles of coordination chemistry, homogeneous catalysis, supramolecular chemistry with the advantages of uniform spatial distribution of catalytic centers, their accessibility and reliable stabilization. This work demonstrates the effectiveness of this approach to the creation of the catalytic composite exhibiting high activity and selectivity in the hydrogenation of LA to GVL. The resulting Ru-containing catalysts with a layer of the pyridylphenylene polymer applied to SiO_2 provided a quantitative yield of GVL. While the pyridine units included in the polymer layer reliably stabilized the Ru^{3+} compounds, the inorganic support, which was a mesoporous silica gel with incorporated iron oxide nanoparticles, provided the possibility to carry out the catalytic reactions in water, due to the presence of hydroxy groups on the surface of silica, gel as well as efficient catalyst separation and recycling. Owing to the reliable stabilization, the ruthenium particles did not aggregate during catalytic tests, and the catalyst maintained its high activity in six catalytic runs.

Acknowledgements

This work was supported by the Russian Science Foundation (project no. 22-43-02025).

S.A.S. is grateful to the Russian Federation President Fellowship for young scientists (No. SP-4370.2021.1).

Corresponding author

* E-mail: shifrina@ineos.ac.ru. Tel: +7(499)135-9355 (Z. B. Shifrina)

Electronic supplementary information

Electronic supplementary information (ESI) available online: scheme for the synthesis of the hybrid organic–inorganic catalyst SiO_2–Fe_3O_4–HPP–Ru; liquid nitrogen adsorption–desorption and X-ray powder diffraction data; comparative data on the catalytic activity of different catalysts in the hydrogenation of LA. For ESI, see DOI: 10.32931/io2320a.

References

1. E. D. Goodman, C. Zhou, M. Cargnello, *ACS Cent. Sci.*, **2020**, *6*, 1916–1937. DOI: 10.1021/acscentsci.0c01046
2. A. Erigoni, U. Diaz, *Catalysts*, **2021**, *11*, 79. DOI: 10.3390/catal11010079
3. J.-M. García-Martínez, E. P. Collar, *Polymers*, **2021**, *13*, 86. DOI: 10.3390/polym13010086
4. A. P. Wight, M. E. Davis, *Chem. Rev.*, **2002**, *102*, 3589–3614. DOI: 10.1021/cr010334m
5. A. Coloma, A. Velty, U. Díaz, *RSC Adv.*, **2023**, *13*, 10144–10156. DOI: 10.1039/D3RA01486J
6. Y. Long, Z. Zhao, L. Wu, S. Luo, H. Wen, W. Wu, H. Zhang, J. Ma, *Mol. Catal.*, **2017**, *433*, 291–300. DOI: 10.1016/j.mcat.2017.02.028
7. K. Motokura, M. Ikeda, M. Nambo, W.-J. Chun, K. Nakajima, S. Tanaka, *ChemCatChem*, **2017**, *9*, 2924–2929. DOI: 10.1002/cctc.201700439
8. H. Yan, H. Cheng, H. Yi, Y. Lin, T. Yao, C. Wang, J. Li, S. Wei, J. Lu, *J. Am. Chem. Soc.*, **2015**, *137*, 10484–10487. DOI: 10.1021/jacs.5b06485
9. X. Yan, P. Duan, F. Zhang, H. Li, H. Zhang, M. Zhao, X. Zhang, B. Xu, S. J. Pennycook, J. Guo, *Carbon*, **2019**, *143*, 378–384. DOI: 10.1016/j.carbon.2018.11.021
10. Z. Wu, X. Zhang, E. D. Goodman, W. Huang, A. R. Riscoe, S. Yacob, M. Cargnello, *ACS Catal.*, **2020**, *10*, 9356–9365. DOI: 10.1021/acscatal.0c01863
11. S. Ji, Y. Chen, X. Wang, Z. Zhang, D. Wang, Y. Li, *Chem. Rev.*, **2020**, *120*, 11900–11955. DOI: 10.1021/acs.chemrev.9b00818
12. R. Lang, X. Du, Y. Huang, X. Jiang, Q. Zhang, Y. Guo, K. Liu, B. Qiao, A. Wang, T. Zhang, *Chem. Rev.*, **2020**, *120*, 11986–12043. DOI: 10.1021/acs.chemrev.0c00797
13. M. Nemanashi, J.-H. Noh, R. Meijboom, *Appl. Catal.*, *A*, **2018**, *550*, 77–89. DOI: 10.1016/j.apcata.2017.10.015
14. J. Min, C. Ma, X. Liu, J. Li, H. Jiang, X. Wen, X. Chen, E. Mijowska, T. Tang, *ACS Omega*, **2018**, *3*, 17573–17580. DOI: 10.1021/acsomega.8b01587
15. F. Giacalone, V. Campisciano, C. Calabrese, V. La Parola, Z. Syrgiannis, M. Prato, M. Gruttadauria, *ACS Nano*, **2016**, *10*, 4627–4636. DOI: 10.1021/acsnano.6b00936
16. B. Wang, Y. Li, Q. Zhu, J. Zhu, Z. Zhang, J. Ma, *Catal. Sci. Technol.*, **2023**, *13*, 887–897. DOI: 10.1039/D2CY01784A
17. E. Karakhanov, A. Maximov, Y. Kardasheva, V. Semernina, A. Zolotukhina, A. Ivanov, G. Abbott, E. Rosenberg, V. Vinokurov, *ACS Appl. Mater. Interfaces*, **2014**, *6*, 8807–8816. DOI: 10.1021/am501528a
18. Q. Wang, Y. Zhang, Y. Zhou, Z. Zhang, Y. Xu, C. Zhang, X. Sheng, *New J. Chem.*, **2015**, *39*, 9942–9950. DOI: 10.1039/C5NJ02318A
19. D. Wang, C. Deraedt, L. Salmon, C. Labrugère, L. Etienne, J. Ruiz, D. Astruc, *Chem. Eur. J.*, **2015**, *21*, 1508–1519. DOI: 10.1002/chem.201404590
20. Z. B. Shifrina, M. S. Rajadurai, N. V. Firsova, L. M. Bronstein, X. Huang, A. L. Rusanov, K. Muellen, *Macromolecules*, **2005**, *38*, 9920–9932. DOI: 10.1021/ma051802n
21. N. V. Kuchkina, S. A. Sorokina, A. V. Bykov, M. G. Sulman, L. M. Bronstein, Z. B. Shifrina, *Nanomaterials*, **2021**, *11*, 3345. DOI: 10.3390/nano11123345
22. N. V. Kuchkina, S. A. Sorokina, B. P. Lawson, A. S. Torozova, L. Zh. Nikoshvili, E. M. Sulman, O. L. Lependina, B. D. Stein, M. Pink, D. G. Morgan, L. M. Bronstein, Z. B. Shifrina, *React. Funct. Polym.*, **2020**, *151*, 104582. DOI: 10.1016/j.reactfunctpolym.2020.104582
23. S. A. Sorokina, N. V. Kuchkina, B. P. Lawson, I. Yu. Krasnova, N. A. Nemygina, L. Zh. Nikoshvili, V. N. Talanova, B. D. Stein, M. Pink, D. G. Morgan, E. M. Sulman, L. M. Bronstein, Z. B. Shifrina, *Appl. Surf. Sci.*, **2019**, *488*, 865–873. DOI: 10.1016/j.apsusc.2019.05.141
24. N. V. Kuchkina, A. K. Haskell, S. A. Sorokina, A. S. Torozova, L. Zh. Nikoshvili, E. M. Sulman, B. D. Stein, D. G. Morgan, L. M. Bronstein, Z. B. Shifrina, *ACS Appl. Mater. Interfaces*, **2020**, *12*, 22170–22178. DOI: 10.1021/acsami.0c04357
25. S. A. Sorokina, N. V. Kuchkina, M. E. Grigoriev, A. V. Bykov, A. K. Ratnikov, V. Yu. Doluda, M. G. Sulman, Z. B. Shifrina, *Catalysts*, **2023**, *13*, 1. DOI:10.3390/catal13010001
26. S. Kang, J. Fu, G. Zhang, *Renew. Sustainable Energy Rev.*, **2018**, *94*, 340–362. DOI: 10.1016/j.rser.2018.06.016
27. W.-P. Xu, X.-F. Chen, H.-J. Guo, H.-L. Li, H.-R. Zhang, L. Xiong, X.-D. Chen, *J. Chem. Technol. Biotechnol.*, **2021**, *96*, 3009–3024. DOI: 10.1002/jctb.6810
28. K. Yan, C. Jarvis, J. Gu, Y. Yan, *Renewable Sustainable Energy Rev.*, **2015**, *51*, 986–997. DOI: 10.1016/j.rser.2015.07.021
29. S. Dutta, I. K. M. Yu, D. C. W. Tsang, Y. H. Ng, Y. S. Ok, J. Sherwood, J. H. Clark, *Chem. Eng. J.*, **2019**, *372*, 992–1006. DOI: 10.1016/j.cej.2019.04.199
30. K. Yan, Y. Yang, J. Chai, Y. Lu, *Appl. Catal.*, *B*, **2015**, *179*, 292–304. DOI: 10.1016/j.apcatb.2015.04.030
31. K. Murugesan, A. S. Alshammari, M. Sohail, R. V. Jagadeesh, *ACS Sustainable Chem. Eng.*, **2019**, *7*, 14756–14764. DOI: 10.1021/acssuschemeng.9b02692
32. Y. Liu, Q. Xin, D. Yin, S. Liu, L. Li, C. Xie, S. Yu, *Catal. Lett.*, **2020**, *150*, 3437–3446. DOI: 10.1007/s10562-020-03245-5
33. D. He, Q. He, P. Jiang, G. Zhou, R. Hu, W. Fu, *Catal. Commun.*, **2019**, *125*, 82–86. DOI: 10.1016/j.catcom.2019.03.029
34. S. Song, S. Yao, J. Cao, L. Di, G. Wu, N. Guan, L. Li, *Appl. Catal.*, *B*, **2017**, *217*, 115–124. DOI: 10.1016/j.apcatb.2017.05.073
35. D. Yanase, R. Yoshida, S. Kanazawa, Y. Yamada, S. Sato, *Catal. Commun.*, **2020**, *139*, 105967. DOI: 10.1016/j.catcom.2020.105967
36. A. L. Maximov, A. V. Zolotukhina, A. A. Mamedli, L. A. Kulikov, E. A. Karakhanov, *ChemCatChem*, **2018**, *10*, 222–233. DOI: 10.1002/cctc.201700691
37. X. Gao, S. Zhu, M. Dong, J. Wang, W. Fan, *Appl. Catal.*, *B*, **2019**, *259*, 118076. DOI: 10.1016/j.apcatb.2019.118076
38. Z. Ruiz-Bernal, M. Á. Lillo-Ródenas, M. del Carmen Román-Martínez, *Catalysts*, **2021**, *11*, 559. DOI: 10.3390/catal11050559
39. T. Oracko, R. Jaquish, Y. B. Losovyj, D. G. Morgan, M. Pink, B. D. Stein, V. Yu. Doluda, O. P. Tkachenko, Z. B. Shifrina, M. E. Grigoriev, A. I. Sidorov, E. M. Sulman, L. M. Bronstein, *ACS Appl. Mater. Interfaces*, **2017**, *9*, 34005–34014. DOI: 10.1021/acsami.7b11643

40. K. Park, S. Padmanaban, S.-H. Kim, K.-D. Jung, S. Yoon, *ChemCatChem*, **2021**, *13*, 695–703. DOI: 10.1002/cctc.202001376
41. D. J. Morgan, *Surf. Interface Anal.*, **2015**, *47*, 1072–1079. DOI: 10.1002/sia.5852
42. M. M. T. Khan, G. Ramachandraiah, R. S. Shukla, *Inorg. Chem.*, **1988**, *27*, 3274–3278. DOI: 10.1021/ic00292a006
43. S. Gundekari, K. Srinivasan, *Appl. Catal.*, *A*, **2019**, *569*, 117–125. DOI: 10.1016/j.apcata.2018.10.018